Single-nano region metastable clustering in this study was confirmed by scanning probe microscopy (SPM), as shown in Fig. 8. Dilute solutions of $C_{60}(OH)_{36}$ at various concentrations (A: (EtOH/water = 0/100; single molecular dispersion), B: (30/70; metastable cluster) and C: (80/20; secondary aggregation)) were applied to a mica plate and dried for SPM observation (Liu et al. 2011). Height measurements for each sample revealed cluster sizes (ca. 1 nm for A, 6–8 nm for B and 18–28 nm for C) that were consistent with those obtained via the IG method (Fig. 9).

Conclusions

Magic number effects were observed by IG and SPM analysis for the formation of metastable clusters with a particle diameter of ca. 6–8 nm of highly polyhydroxylated fullerenol $C_{60}(OH)_{36}$ in water–alcohol binary solvent, whereas such aggregation behaviours were not found in DMSO–alcohol binary system or for the less hydroxylated fullerenol $C_{60}(OH)_{10}$.

Acknowledgments This study was supported by JSPS KAKENHI of a Grant-in-Aid for Challenging Exploratory Research No. 23651111 and by Health Labour Sciences Research Grants from MHLW of Japan. The authors thank Shimadzu Corporation for collaborative measurements on IG and SPM analysis.

References

Anagnostatos GS (1987) Magic numbers in small clusters of rare-gas and alkali atoms. Phys Lett A 124:85–89

Bhuiyan MMH, Ferdaush J, Uddin MH (2007) Density and viscosities of binary mixtures of dimethylsulfoxide + aliphatic lower alkanols (C1–C3) at temperatures from T = 303.15 K to T = 323.15 K. J Chem Thermodyn 39:675–683

Boyen H-G, Kästle G, Weigl F, Koslowski B, Dietrich C, Ziemann P, Spats JP, Riethmüller S, Hartmann C, Möller M, Schmid G, Garnier MG, Oelhafen P (2002) Oxidation-resistant gold-55 clusters. Science 297:1533–1536

Brant J, Lecoanet H, Wiesner MR (2005) Aggregation and deposition characteristics of fullerene nanoparticles in aqueous systems. J Nanopart Res 7:545–553

Branz W, Malinowski N, Enders A, Martin TP (2002) Structural transition on $(C_{60})_n$ clusters. Phys Rev B 66:094107

Chae S-R, Hotze EM, Wiesner MR (2009) Evaluation of the oxidation of organic compounds by aqueous suspensions of photosensitized hydroxylated-C_{60} fullerene aggregates. Environ Sci Technol 43:6208–6213

Deguchi S, Mukai S, Tsudome M, Horikoshi K (2006) Facile generation of fullerene nanoparticles by hand-grinding. Adv Mater 18:729–732

Garvey JF, Herron WJ, Vaidyanathan G (1994) Probing the structure and reactivity of hydrogen-bonded clusters of the type $\{M\}_n\{H_2O\}H^+$, via the observation of magic numbers. Chem Rev 94:1999–2014

González B, Calvar N, Gómez E, Domínguez Á (2007) Density, dynamic viscosity, and derived properties of binary mixtures of methanol or ethanol with water, ethyl acetate, and methyl acetate at T = (293.15, 298.15, and 303.15) K. J Chem Thermodyn 39:1578–1588

Grande MdC, García M, Marschoff CM (2009) Density and viscosity of anhydrous mixtures of dimethylsulfoxide with acetonitrile in the range (298.15 to 318.15) K. J Chem Eng Data 54:652–658

Hansen K, Hohmann H, Müller R, Campbell EEB (1996) Icosahedra of icosahedra: the stability of $(C_{60})_{13}$. J Chem Phys 105:6088–6089

Kokubo K, Matsubayashi K, Tategaki H, Takada H, Oshima T (2008) Facile synthesis of highly water-soluble fullerenes more than half-covered by hydroxyl groups. ACS Nano 2:327–333

Kokubo K, Shirakawa S, Kobayashi N, Aoshima H, Oshima T (2011) Facile and scalable synthesis of a highly hydroxylated water-soluble fullerenol as a single nanoparticle. Nano Res 4:204–215

Kyzyma OA, Korobov MV, Avdeev MV, Garamus VM, Snegir SV, Petrenko VI, Aksenov VL, Bulavin LA (2010) Aggregate development in C_{60}/*N*-methyl-2-pyrrolidone solution and its mixture with water as revealed by extraction and mass spectroscopy. Chem Phys Lett 493:103–106

Liu Y, Zhang G, Niu L, Gan L, Liang D (2011) Assembly of Janus fullerenol: a novel approach to prepare rich carbon structures. J Mater Chem 21:14864–14868

Martin TP, Näher P, Schaber H, Zimmermann U (1993) Clusters of fullerene molecules. Phys Rev Lett 70:3079–3082

Mikhail SZ, Kimel WR (1963) Densities and viscosities of 1-propanol–water mixtures. J Chem Eng Data 8:323–328

Mohan H, Palit DK, Mittal JP, Chiang LY, Asmus K-D, Guldi DM (1998) Excited states and electron transfer reactions of $C_{60}(OH)_{18}$ in aqueous solution. J Chem Soc Faraday Trans 94:359–363

Nath S, Pal H, Palit DK, Sapre AV, Mittal JP (1998) Aggregation of fullerene, C_{60}, in benzonitrile. J Phys Chem B 102:10158–10164

Rodríguez-Zavala JG, Barajas-Barraza RE, Padilla-Osuna I, Guirado-López RA (2011) Hydration behaviour of polyhydroxylated fullerenes. J Phys B 44:205104–205117

Sakurai M, Watanabe K, Sumiyama K, Suzuki K (1999) Magic numbers in transition metal (Fe, Ti, Zr, Nb, and Ta) clusters observed by time-of flight mass spectrometry. J Chem Phys 111:235–238

Sattler K (1993) C_{60} and beyond: from magic numbers to new materials. Jpn J Appl Phys 32:1428–1432

Semenov KN, Charykov NA, Keskinov VN (2011) Fullerenol synthesis and identification. Properties of the fullerenol water solution. J Chem Eng Data 56:230–239

Wada Y, Totoki S, Watanabe M, Moriya N, Tsunazawa Y, Shimaoka H (2006) Nanoparticle size analysis with

relaxation of induced grating by dielectrophoresis. Opt Express 14:5755–5764

Wakisaka A, Komatsu S, Usui Y (2001) Solute–solvent and solvent–solvent interactions evaluated through clusters isolated from solutions: preferential solvation in water–alcohol mixtures. J Mol Liq 90:175–184

Ying Q, Marecek J, Chu B (1994) Slow aggregation of buckminsterfullerene (C_{60}) in benzene solution. Chem Phys Lett 219:214–218

Young LDR, Fink AL, Dill KA (1993) Aggregation of globular proteins. Acc Chem Res 26:614–620

ChemComm

RSC Publishing

COMMUNICATION

Ionic conductivity of $[Li^+@C_{60}](PF_6^-)$ in organic solvents and its electrochemical reduction to $Li^+@C_{60}^{\bullet-}$

Cite this: *Chem. Commun.*, 2013, **49**, 7376

Received 24th May 2013,
Accepted 26th June 2013

DOI: 10.1039/c3cc43901a

www.rsc.org/chemcomm

Hiroshi Ueno,[a] Ken Kokubo,*[a] Yuji Nakamura,[a] Kei Ohkubo,[b] Naohiko Ikuma,[a] Hiroshi Moriyama,[c] Shunichi Fukuzumi[bd] and Takumi Oshima[a]

The ionic conductivity of $[Li^+@C_{60}](PF_6^-)$ was measured in *o*-dichlorobenzene, and found to be higher than that of $TBA^+PF_6^-$. Electrochemical reduction of $[Li^+@C_{60}](PF_6^-)$ without any supporting electrolyte gave the monovalent radical anion $Li^+@C_{60}^{\bullet-}$, as confirmed by the characteristic ESR signal and NIR absorption band.

Lithium-cation-encapsulated [60]fullerene $Li^+@C_{60}$, which was first isolated as the $[Li^+@C_{60}](SbCl_6^-)$ salt, is the only known endohedral metallo[60]fullerene with 100% encapsulation ratio, and its structure has been established by single crystal X-ray analysis.[1–3] It has attracted growing attention because of its unique properties such as stronger electron acceptability than pristine C_{60} and high reactivities in photoinduced electron transfer and regioselective multihydroxylation.[4–8] The most remarkable property of the $[Li^+@C_{60}]$ salt is its high ionicity resulting from the encapsulated lithium cation. Although this ionic nature of $[Li^+@C_{60}](PF_6^-)$ is stated to be responsible for its rock-salt-type crystal structure,[2] no other details of the effects of ionicity have been reported so far.

The fullerene radical anion has been recognised as an intriguing material because of its unique electronic properties such as (super)conductivity and ferromagnetism.[9–12] In addition, the radial anion can serve as an important reaction intermediate for various unique chemical modifications of the fullerene cage.[13] Although many methods for the preparation of empty C_{60} radical anion salts have been reported,[14] studies on endohedral fullerene radical anions are relatively stagnant.

We herein report the high ionic conductivity of $[Li^+@C_{60}](PF_6^-)$ in organic solvents, which has enabled a facile electrochemical synthesis of the radical anion $(Li^+@C_{60}^{\bullet-})$ without any supporting electrolyte.

The ionic conductivity measurements were performed in *o*-dichlorobenzene (*o*-DCB) and benzonitrile (PhCN) since $[Li^+@C_{60}](PF_6^-)$ showed sufficient solubility and electrochemical stability in these solvents.† The molar conductivity Λ is defined in eqn (1), where κ is the measured conductivity at each concentration (c). The Λ values for various concentrations

$$\Lambda = \kappa/c \quad (1)$$

of $[Li^+@C_{60}](PF_6^-)$ are shown in Fig. 1 and listed in Table 1, together with those of tetra-*n*-butylammonium hexafluorophosphate ($TBA^+PF_6^-$), which is commonly used as a supporting electrolyte in organic solvents. The exponential change in Λ with $c^{1/2}$ indicated that $[Li^+@C_{60}](PF_6^-)$ itself acted as a supporting electrolyte. As pristine C_{60} showed no ionic conductivity under the same conditions, the observed conductivity was regarded as a unique feature of the ion-encapsulated fullerene. The observed

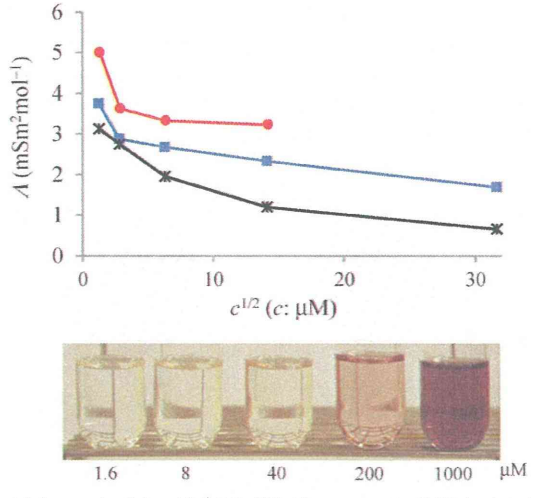

Fig. 1 Molar conductivity of $[Li^+@C_{60}](PF_6^-)$ measured in PhCN (red circles) and *o*-DCB (blue squares) solutions containing various concentrations of $[Li^+@C_{60}](PF_6^-)$ at 298 K. The black line is the result of $TBA^+PF_6^-$ measured as a reference (asterisks). The picture shows the various concentrations of $[Li^+@C_{60}](PF_6^-)$ in *o*-DCB solutions.

[a] *Division of Applied Chemistry, Graduate School of Engineering, Osaka University, 2-1 Yamadaoka, Suita, Osaka 565-0871, Japan. E-mail: kokubo@chem.eng.osaka-u.ac.jp; Fax: +81-6-6879-4593; Tel: +81-6-6879-4592*

[b] *Department of Material and Life Science, Graduate School of Engineering, Osaka University, and ALCA, Japan Science and Technology (JST), Suita, Osaka 565-0871, Japan*

[c] *Department of Chemistry, Faculty of Science, Toho University, 2-2-1 Miyama, Funabashi, Chiba 274-8510, Japan*

[d] *Department of Bioinspired Science, Ewha Womans University, Seoul, 120-750, Korea*

Table 1 Ionic conductivities of $[Li^+@C_{60}](PF_6^-)$ and $TBA^+PF_6^-$ measured in *o*-DCB at 298.0 K

c/μM	κ/mS m^{-1}	Λ/mS m^{-2} mol^{-1}
$[Li^+@C_{60}](PF_6^-)$		
1.6	0.006 (0.008)[a]	3.75 (5.00)[a]
8	0.023 (0.029)[a]	2.88 (3.63)[a]
40	0.107 (0.133)[a]	2.68 (3.33)[a]
200	0.466 (0.646)[a]	2.33 (3.23)[a]
1000	1.688 (—[b])[a]	1.69 (—[b])[a]
$TBA^+PF_6^-$		
1.6	0.005	3.13
8	0.022	2.75
40	0.078	1.95
200	0.238	1.19
1000	0.649	0.50
Pristine C_{60}		
Any	0.000	0.00

[a] Values in parentheses are measured in PhCN. [b] Not determined due to the solubility limitation.

ionic conductivity of $[Li^+@C_{60}](PF_6^-)$ was higher than that of $TBA^+PF_6^-$, indicating the weak interaction between the counter anion PF_6^- and encapsulated Li^+ even in such less polar solvents.

To discuss the ionizability of $[Li^+@C_{60}](PF_6^-)$, the electrostatic potential of the $[Li^+@C_{60}]$ cation and the distance between the cation and the PF_6^- anion at the most stable position were calculated by the density functional theory (DFT) at the B3LYP/6-31G* level. The result showed that the positive charge of the $[Li^+@C_{60}]$ cation was not only located on the encapsulated Li^+ but also strongly delocalised on the carbon atoms of the C_{60} cage. Because of the thermal motion of the encapsulated Li^+ in the C_{60} cage, the charge delocalization might be more dynamically significant.[2] Furthermore, the Li–P distance of $[Li^+@C_{60}](PF_6^-)$ was calculated to be 5.65 Å, which was much longer than that in $LiPF_6$ (2.63 Å). This difference implied that the positional relationship observed between Li^+ and PF_6^- in $[Li^+@C_{60}](PF_6^-)$ is unusual in common ion pairs, indicating that the electrostatic attractive force between the $[Li^+@C_{60}]$ cation and PF_6^- is weak due to the delocalised positive charge on the C_{60} cage and the distance limitation by this cage. This result is consistent with the previous report that the encapsulated Li^+ is in thermal motion at around room temperature even if the $[Li^+@C_{60}]$ cation forms an ion pair with PF_6^-.[2]

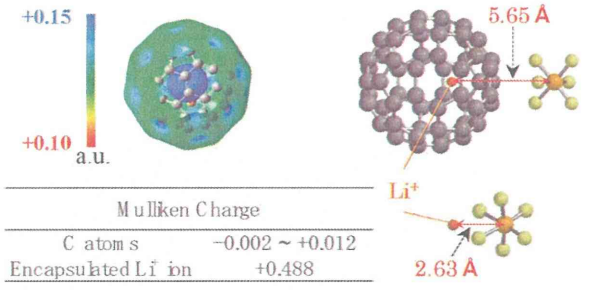

Fig. 2 Electrostatic potential of the $[Li^+@C_{60}]$ cation and the distance between encapsulated Li^+ and outer PF_6^- obtained by the theoretical calculation (B3LYP/6-31G* method), the distances between Li^+ and P for $Li^+@C_{60}$ and $LiPF_6$, and the Mulliken charges on C and Li^+ atoms of the $[Li^+@C_{60}]$ cation.

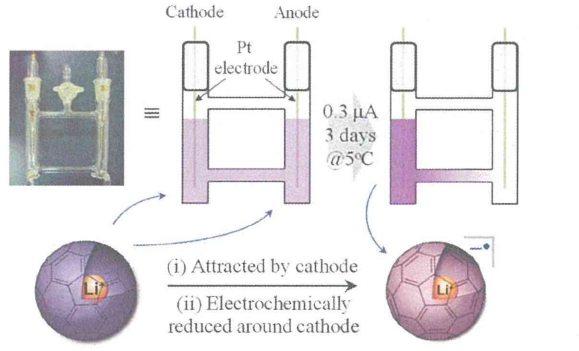

Fig. 3 Pattern diagram of the electrochemical synthesis of $Li^+@C_{60}^{\bullet-}$.

Moreover, the solvation effect is also important for the ion pair formation.[15] Because C_{60} is a π-conjugated molecule, there must be strong π–π interaction between the cage and the aromatic solvent molecules, and the solvation can stabilize the ionized $[Li^+@C_{60}]$ cation.[16] Thus, $[Li^+@C_{60}](PF_6^-)$ tends to ionize, showing ionic conductivity, to be used as a unique electrolyte which, despite its high ionicity, can be used in low-polarity aromatic solvents. Incidentally, the higher value of Λ in PhCN than that in *o*-DCB was explained by the difference in the relative permittivity (ε_r) between PhCN (ε_r = 25.2) and *o*-DCB (9.93).[17]

Based on the above results, we attempted at synthesis of the Li^+-encapsulated fullerene radical anion electrochemically without using any supporting electrolyte. All the synthetic process was carried out under N_2 atmosphere. The synthetic scheme is shown in Fig. 3. An *o*-DCB solution of $[Li^+@C_{60}](PF_6^-)$ (0.25 mg mL^{-1}, 0.29 μM) was set in an H-type cell, cooled to 278 K, and electrolyzed using a Pt electrode at a constant current (0.3 μA) for 3–4 days. The homogeneous purple solution gradually became gradated because of ion conduction by the $[Li^+@C_{60}]$ cation and PF_6^-. The cation was electrochemically reduced at the cathode, and a monovalent radical anion of Li^+-encapsulated fullerene $Li^+@C_{60}^{\bullet-}$ was selectively formed.

The generated $Li^+@C_{60}^{\bullet-}$ was characterised by UV-vis-NIR and ESR spectroscopy. ^7Li and ^{13}C NMR, dynamic light scattering (DLS), and ζ potential distribution measurements did not furnish meaningful signals/results, probably because of the low concentration of the target species, in addition to paramagnetic relaxation. The UV-vis-NIR spectra of the solution collected from the cathode side after 3 days are shown in Fig. 4, along with the spectrum of the starting $[Li^+@C_{60}](PF_6^-)$ solution. The absorption maximum observed at 1035 nm was clearly assignable to the monovalent radical anion of the Li^+-encapsulated C_{60}.[7,8] The generation of $Li^+@C_{60}^{\bullet-}$ was also confirmed by the ESR spectrum (Fig. 5). The observed g value (2.00058) clearly indicated that the monovalent radical anion was exclusively produced through one-electron reduction. At 77 K, the thermal motion of the encapsulated Li^+ may stop, and thus, the spectrum showed a sharp signal. The calculated spin density of $Li^+@C_{60}^{\bullet-}$ for the optimised structure indicated that the delocalised spin density is somewhat close to the encapsulated Li^+. However, because of the small hyperfine coupling constant of the Li species, the interaction between the encapsulated Li^+ and

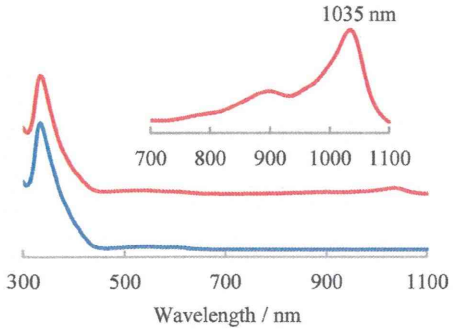

Fig. 4 UV-vis-NIR absorption spectra of the product solution by electrochemical reduction of $[Li^+@C_{60}](PF_6^-)$ (red line) and starting $[Li^+@C_{60}](PF_6^-)$ solution (blue line) in *o*-DCB. The inset shows the expanded view of the NIR region of the spectrum of the product.

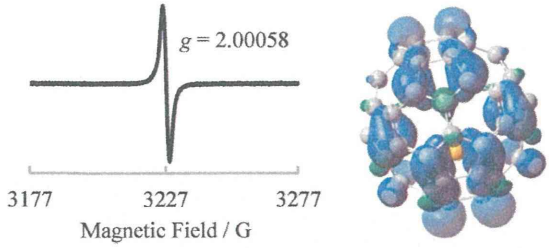

Fig. 5 ESR spectrum of the product measured at 77 K (left) and calculated spin density (B3LYP/6-31G* method) of $Li^+@C_{60}^{\bullet-}$ in the optimised structure (right).

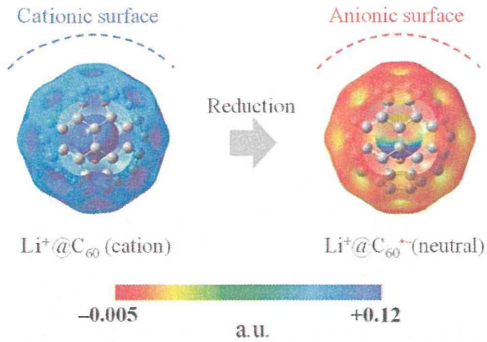

Fig. 6 Calculated electrostatic potential (B3LYP/6-31G* method) of $Li^+@C_{60}$ (left) and $Li^+@C_{60}^{\bullet-}$ (right). The left figure is different from Fig. 2 only in the potential range. $Li^+@C_{60}^{\bullet-}$ had a slightly negative potential on the C_{60} cage (~0.022). In order to simplify the map, the range was set in +0.002 to +0.12.

the spin centre could not be evidenced from the spectrum. Although the ζ potentials of the starting $[Li^+@C_{60}](PF_6^-)$ and the resulting $Li^+@C_{60}^{\bullet-}$ could not be compared because of the above reasons, the two species could be clearly distinguished from each other on the basis of the calculated electrostatic potential (Fig. 6). This result indicated that the chemical reactivities of the two types of Li^+-encapsulated fullerenes, the external-counter-anion-type $[Li^+@C_{60}](PF_6^-)$ and the cation-encapsulated-anion-type $Li^+@C_{60}^{\bullet-}$, are much different, and hence, $Li^+@C_{60}^{\bullet-}$ is a potential nucleophilic reactant for unique chemical transformations.

In conclusion, the ionic conductivity of Li^+-encapsulated [60]fullerene $[Li^+@C_{60}](PF_6^-)$ was measured in two organic solvents, *o*-DCB and PhCN. $[Li^+@C_{60}](PF_6^-)$ showed higher ionic conductivity than $TBA^+PF_6^-$, indicating the possibility of electrochemical applications even in the absence of any supporting electrolyte. Furthermore, the Li^+-encapsulated [60]fullerene monovalent radical anion $Li^+@C_{60}^{\bullet-}$ was synthesised selectively by a very facile electrochemical method. Further studies on the use of anion-exchanged $[Li^+@C_{60}]$, application of $[Li^+@C_{60}](PF_6^-)$ as a unique electrolyte, and derivatisation *via* the anion species are now in progress, in addition to the synthesis and characterization of multivalent anions.

This work was supported by Grant-in-Aid for Exploratory Research (No. 23651111 to K.K.; No. 23750014 to K.O.; No. 23550211 to H.M. & 23108010 to S.F.) from JSPS, Japan, Health Labour Sciences Research Grants from MHLW, Japan, and a WCU project (R31-2008-000-10010-0) through KOSEF/MEST, Korea.

References

† General procedure: $[Li^+@C_{60}](PF_6^-)$ was obtained from Idea International Corporation and purified by recrystallization from chlorobenzene/acetonitrile. All other reagents were commercially available and used without further purification. Ionic conductivity measurement was performed using a HORIBA ES-51 under N_2 atmosphere. UV-vis-NIR spectra were recorded on a Shimadzu UV-1800 spectrometer. The ESR spectrum was measured on a JEOL JES-FA100. A YAZAWA CS-12Z constant current regulator was used for electrochemical synthesis of $Li^+@C_{60}^{\bullet-}$.

1 S. Aoyagi, E. Nishibori, H. Sawa, K. Sugimoto, M. Takata, Y. Miyata, R. Kitaura, H. Shinohara, H. Okada, T. Sakai, Y. Ono, K. Kawachi, K. Yokoo, S. Ono, K. Omote, Y. Kasama, S. Ishikawa, T. Komuro and H. Tobita, *Nat. Chem.*, 2010, **2**, 678.
2 S. Aoyagi, Y. Sado, E. Nishibori, H. Sawa, H. Okada, H. Tobita, Y. Kasama, R. Kitaura and H. Shinohara, *Angew. Chem., Int. Ed.*, 2012, **51**, 3377.
3 H. Okada, T. Komuro, T. Sakai, Y. Matsuo, Y. Ono, K. Omote, K. Yokoo, K. Kawachi, Y. Kasama, S. Ono, R. Hatakeyama, T. Kaneko and H. Tobita, *RSC Adv.*, 2012, **2**, 10624.
4 H. Ueno, Y. Nakamura, N. Ikuma, K. Kokubo and T. Oshima, *Nano Res.*, 2012, **6**, 558.
5 H. Ueno, K. Kokubo, E. Kwon, Y. Nakamura, N. Ikuma and T. Oshima, *Nanoscale*, 2013, **5**, 2317.
6 Y. Matsuo, H. Okada, M. Maruyama, H. Sato, H. Tobita, Y. Ono, K. Omote, K. Kawachi and Y. Kasama, *Org. Lett.*, 2012, **14**, 3784.
7 S. Fukuzumi, K. Ohkubo, Y. Kawashima, D. S. Kim, J. S. Park, A. Jana, V. M. Lynch, D. Kim and J. L. Sessler, *J. Am. Chem. Soc.*, 2011, **133**, 15938.
8 (*a*) K. Ohkubo, Y. Kawashima and S. Fukuzumi, *Chem. Commun.*, 2012, **48**, 4314; (*b*) Y. Kawashima, K. Ohkubo and S. Fukuzumi, *J. Phys. Chem. A*, 2012, **116**, 8942.
9 K. Tanigaki, I. Hirosawa, T. W. Ebbesen, J. Mizuki, Y. Shimakawa, Y. Kubo, J. S. Tsai and S. Kuroshima, *Nature*, 1992, **356**, 419.
10 A. Y. Ganin, Y. Takabayashi, P. Jeglič, D. Arčon, A. Potočnik, P. J. Baker, Y. Ohishi, M. T. McDonald, M. D. Tzirakis, A. Mclennan, G. R. Darling, M. Takata, M. J. Rosseinsky and K. Prassides, *Nature*, 2010, **466**, 221.
11 (*a*) H. Moriyama, H. Kobayashi, A. Kobayashi and T. Watanabe, *J. Am. Chem. Soc.*, 1993, **115**, 1185; (*b*) H. Kobayashi, H. Tomita, H. Moriyama, A. Kobayashi and T. Watanabe, *J. Am. Chem. Soc.*, 1994, **116**, 3153; (*c*) H. Moriyama, M. Abe, H. Motoke, T. Watanabe, S. Hayashi and H. Kobayashi, *Synth. Met.*, 1998, **94**, 167.
12 P. W. Stephens, D. Cox, J. W. Lauher, L. Mihaly, J. B. Wiley, P.-M. Allemand, A. Hirsch, K. Holczer, Q. Li, J. D. Thompson and F. Wudl, *Nature*, 1992, **355**, 331.
13 K. Kokubo, R. S. Arastoo, T. Oshima, C. C. Wang, Y. Gao, H. L. Wang, H. Geng and L. Y. Chiang, *J. Org. Chem.*, 2010, **75**, 4574.
14 C. A. Reed and R. D. Bolskar, *Chem. Rev.*, 2010, **100**, 1075.
15 Y. Marcus and G. Hefter, *Chem. Rev.*, 2006, **106**, 4585.
16 T. Oshima, T. Mikie, N. Ikuma and H. Yakuma, *Org. Biomol. Chem.*, 2010, **10**, 1730.
17 H. F. Friedman and B. Larsen, *J. Chem. Phys.*, 1979, **70**, 92.

Bioorganic & Medicinal Chemistry 21 (2013) 7709–7714

Contents lists available at ScienceDirect

Bioorganic & Medicinal Chemistry

journal homepage: www.elsevier.com/locate/bmc

Antioxidant activities of 5-hydroxyoxindole and its 3-hydroxy-3-phenacyl derivatives: The suppression of lipid peroxidation and intracellular oxidative stress

Daisuke Yasuda [a], Kyoko Takahashi [a], Tomoyuki Ohe [a], Shigeo Nakamura [b], Tadahiko Mashino [a,*]

[a] Department of Pharmaceutical Sciences, Faculty of Pharmacy, Keio University, 1-5-30 Shibakoen, Minato-ku, Tokyo, Japan
[b] Department of Chemistry, Nippon Medical School, 2-297-2 Kosugi-cho, Nakahara-ku, Kawasaki-shi, Kanagawa, Japan

ARTICLE INFO

Article history:
Received 20 September 2013
Revised 15 October 2013
Accepted 17 October 2013
Available online 30 October 2013

Keywords:
Antioxidant
Radical scavenging activity
Oxidative stress
5-Hydroxyoxindole
Lipophilicity

ABSTRACT

The antioxidant activities of 5-hydroxyoxindole (**1**) and newly synthesized 3,5-dihydroxy-3-phenacyl-2-oxindole derivatives against rat liver microsome/*tert*-butylhydroperoxide system-induced lipid peroxidation and hydrogen peroxide-induced intracellular oxidative stress were investigated. Compound **1** and its derivatives showed significant suppression of lipid peroxidation and an intracellular oxidative stress. The effects of the more lipophilic derivatives tended to be greater than that of the original compound **1**. The cytotoxicity of all of the oxindole derivatives on human promyelocytic leukemia HL60 cells was lower than that of 2,6-di(*tert*-butyl)-4-hydroxytoluene (BHT), a widely used phenolic antioxidant. These results show that compound **1** and its 3-substituted derivatives could be good lead candidates for future novel antioxidant therapeutics.

1. Introduction

Oxidative stress derived from reactive oxygen species (e.g., superoxide, hydrogen peroxide, hydroxyl radical and peroxynitrite) is implicated in various diseases such as cancer, neurodegenerative diseases, cardiovascular diseases and mitochondrial diseases.[1] Natural antioxidants, including ascorbic acid, α-tocopherol, ubiquinol, uric acid and polyphenols are candidate therapeutic agents for such diseases, and indeed, numerous antioxidants and their analogs have been under investigation for clinical uses. Edaravone (3-methyl-*N*-phenylpyrazolin-5-one) scavenges free radicals such as hydroxyl radical and lipid radicals and protects brain against ischemic lesions after stroke, and it has been shown to improve the clinical outcomes for patients with acute ischemic stroke.[2,3] Edaravone may improve amyotrophic lateral sclerosis (ALS) by decreasing neural oxidative stress.[4] These findings indicate that antioxidants have the potential to serve as novel therapeutic agents that address unmet medical needs. However, the majority of natural antioxidants seemed to be not appropriate for clinical use.[5] Thus, novel antioxidants featuring a variety of chemical structures are needed to develop useful therapeutic agents.

Uric acid (Fig. 1) is an endogenous antioxidant and has been reported to act as a neuroprotective agent against multiple sclerosis and Parkinson's disease.[6–11] However, uric acid is poorly soluble in serum and is a causative compound for gout. In our previous study, simplified analogs of uric acid, with a moiety critical for antioxidant activity, were designed and synthesized, and their radical scavenging activity was investigated.[12] Among the uric acid analogs, 5-hydroxyoxindole (**1**, Fig. 1) showed 15.7-fold stronger 1,1-diphenyl-2-picrylhydrazyl (DPPH) radical scavenging activity than uric acid, and low cytotoxicity in human promyelocytic leukemia HL60 cells. Moreover, the solubility of **1** in phosphate buffered saline was fourfold higher than that of uric acid.

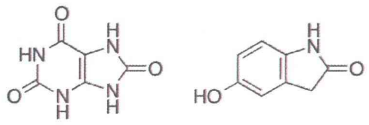

Uric acid 5-Hydroxyoxindole (**1**)

Figure 1. Structures of uric acid and 5-hydroxyoxindole (**1**).

Compound **1** is an endogenous, oxidized indole that was first detected in rat urine.[13] Compound **1** exists at nanomolar levels in the serum and brain of mammals, including humans.[14] Moreover, **1** has shown inhibitory activity toward monoamine oxidase[15] and extracellular signal-related kinase 2 (ERK2).[16] In more recent report, compound **1** has been detected in the cerebrospinal fluid of ewes at different concentrations based on the time and photope-

* Corresponding author. Tel.: +81 3 5400 2694; fax: +81 3 5400 2691.
E-mail address: mashino-td@pha.keio.ac.jp (T. Mashino).

0968-0896/$ - see front matter © 2013 Elsevier Ltd. All rights reserved.
http://dx.doi.org/10.1016/j.bmc.2013.10.021

riod; therefore, **1** has been suggested to be involved in rhythmic adjustments.[17] Although various physiological or biological actions of **1** have been reported, the antioxidant activities of **1** in biological components, such as lipids or cells, have never been investigated. Herein, the antioxidant potential of **1** was evaluated in more detail.

Because the various biological activities of **1** may cause adverse effects, appropriate synthetic modification of **1** was necessary. The lipophilicity of antioxidant molecules is one of the most common and important factors to control the antioxidant effect against lipid peroxidation. Therefore, the introduction of lipophilic substituents on **1** was accomplished to increase its antioxidant effects on biological components. To avoid decreasing the radical scavenging activity by structural modification, we assumed that the C3-position of **1** was suitable for lipophilic substitution. The C3-position of **1** was not deemed critical to radical scavenging activity according to our proposed mechanism[12] because it is an sp^3 carbon, which will not conjugate with the phenolic moiety.

The isatin-based aldol reaction with acetophenones is a typical reaction to obtain 3-disubstituted oxindole derivatives.[18,19] Using this method, the preparation of 3,5-dihydroxy-3-phenacyl-2-oxindole derivatives was performed easily. In this study, various *para*-substituted phenacyl groups were introduced at the C3-position of **1** to control the lipophilicity and antioxidant activities of the newly synthesized analogs, and these compounds were then evaluated.

2. Results

2.1. Synthesis

5-Hydroxyisatin was prepared by the O-demethylation of commercially available 5-methoxyisatin (Scheme 1). All of the 3,5-dihydroxyoxindole derivatives (**2** and **3a–j**) were newly synthesized using an aldol reaction of 5-hydroxyisatin with either acetone or the corresponding *para*-substituted acetophenones in the presence of diethylamine. All of the newly synthesized compounds were characterized by ^1H NMR, ^{13}C NMR and high-resolution mass spectrometry.

2.2. DPPH radical scavenging activity

The DPPH radical scavenging assay is one of the simplest methods to evaluate the reactivity of antioxidants with free radicals in vitro. The radical scavenging activity was expressed as a second-order rate constant between the test compound and DPPH. As shown in Table 1, compound **1** showed higher DPPH radical scavenging activity than uric acid. Derivatives **2** and **3a–j** also showed greater activity than uric acid; however, the activities were lower than that of **1**. The activity of **2** was the weakest among the oxindole derivatives. The activities of **3a–j** were similar with respect to each other.

2.3. Lipid peroxidation inhibitory activity

The inhibitory activity against rat liver microsome/*tert*-butylhydroperoxide system-induced lipid peroxidation was evaluated by the TBARS (thiobarbituric acid reactive substances) method. As shown in Table 1, compound **1** exhibited greater activity than uric acid. The activity of **2** was significantly lower than that of **1**. Derivative **3a–j** showed stronger activity than **1**. The IC_{50} values of **3a–j** for lipid peroxidation ranged from 40 to 240 μM.

2.4. Lipophilicity

The lipophilicities of the oxindole derivatives were measured as an isocratic capacity factor ($\log k_w$ value). The $\log k_w$ value is in good agreement with the octanol–water partition coefficient ($\log P$ value) and is calculated by measuring the retention time on a reverse-phase HPLC using methanol/water as the mobile phase.[20,21] The obtained $\log k_w$ value are listed in Table 1. Derivative **2** exhibited the lowest lipophilicity, and **1** showed the second lowest value. Derivatives **3a–j** had various lipophilicity values, which were greater than the lipophilicity of **1**.

2.5. Intracellular oxidative stress-suppressing effect

The suppressing effect of the oxindole derivatives against H_2O_2-induced intracellular oxidative stress was measured using 2′,7′-dichlorodihydrofluorescin diacetate (DCFH-DA) as a fluorescent probe. DCFH-DA penetrates the cell membrane and then is deacetylated by intracellular esterases to form non-fluorescent 2′,7′-dichlorodihydrofluorescin (DCFH). DCFH is easily oxidized by intracellular ROS to form the fluorescent 2′,7′-dichlorofluorescin (DCF).

H_2O_2 (200 μM) increased the intracellular oxidative stress level compared to the control (Fig. 2). All of the oxindole derivatives except **2** suppressed the oxidative stress level at 10 μM. Derivative **3d** showed the most potent effect, followed by **3g–i**. Uric acid and **2** failed to suppress intracellular oxidative stress.

2.6. Cytotoxicity

The cytotoxicities of the derivatives on HL60 cells were evaluated using a trypan blue dyeexclusion test. In agreement with our previous study,[12] **1** did not show remarkable cytotoxicity at

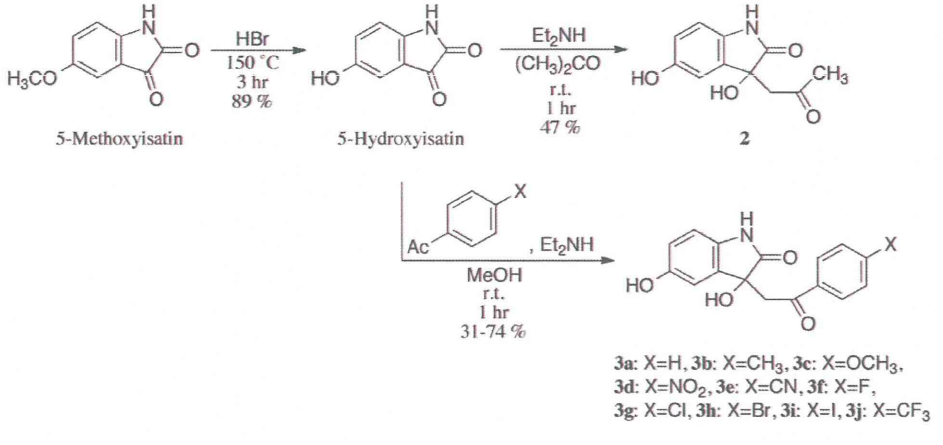

Scheme 1. Synthetic pathways of 3,5-dihydroxyoxindole derivatives.

Table 1
Antioxidant activities and lipophilicity of the oxindole derivatives and uric acid

Compound	DPPH radical scavenging activity ($\times 10^3$ M^{-1} s^{-1})	Lipid peroxidation inhibitory activity (IC_{50}, μM)	Log k_w
1	9.2	300	0.70
2	0.74	>300	0.44
3a	1.9	240	1.07
3b	1.8	160	2.20
3c	1.5	225	1.74
3d	2.5	40	1.85
3e	1.7	150	1.91
3f	1.5	95	1.93
3g	2.4	120	2.45
3h	1.2	75	2.55
3i	2.2	55	2.81
3j	1.6	80	2.89
Uric acid	0.63	>300	Not Tested

100 μM (Fig. 3). Derivatives **2**, **3a–c** also did not show cytotoxicity. On the other hand, derivatives **3e–h** exhibited weak cytotoxicity at 100 μM. 2,6-Di(*tert*-butyl)-4-hydroxytoluene (BHT), a widely used phenolic antioxidant, decreased the cell viability to almost 0%.

3. Discussion

The DPPH radical scavenging activity of **1** was 14.6-fold higher than that of uric acid, which is in good agreement with our previous report.[12] The radical scavenging activity of derivatives **2** and **3a–j** was maintained as expected, but it was lower than the activity of **1** (Table 1). This indicates that introduction of either C3-hydroxy or C3-phenacyl group was the factor to decrease the activity. For the effects of the C3-substituent, especially the consequence of the C3-hydroxy group is under investigation. A substituent at the *para*-position of the phenacyl group scarcely influenced the radical scavenging activity, because the phenacyl group is not conjugated to the oxindole moiety. This phenomenon was supported by the fact that there was no difference among **3a–j** with respect to the ^{1}H NMR chemical shifts corresponding to protons of oxindole moiety (see the Section 5), which suggests that the substituent on the phenacyl group did not affect electronically the oxindole moiety.

In contrast to the results of the DPPH radical scavenging assay, derivative **3a** showed stronger lipid peroxidation inhibitory activity than **1** (Table 1). The inhibitory activity of **2** was lower than that of **1**, as was the case for the radical scavenging assay. These data show that substitution at the 3-position of **1** with a hydroxy and an acetonyl group was ineffective in suppressing lipid peroxidation, but substitution with a hydroxy and a phenacyl group proved to be an effective modification. All oxindole derivatives containing a *para*-substituent on the phenacyl group exhibited stronger inhibitory activity than that of the non-substituted **3a**. The inhibitory activity of **3a–j** was greatly influenced by the substituent on the phenacyl group, which contrasted with the results for the DPPH radical scavenging activity. No correlation was observed between the DPPH radical scavenging activity and the lipid peroxidation inhibitory activity, but the lipophilicity of the oxindole derivatives (Table 1) tended to correlate with the IC_{50} value for lipid peroxidation. The lipid peroxidation inhibitory activity is presumably controlled by the localization of the antioxidants into microsomal membranes. Thus, the present results indicate that the antioxidant capacity of the oxindole derivatives increased because the *para*-substituted phenacyl group increased the lipophilicity of the entire molecule.

The series of oxindole derivatives, except **2**, showed intracellular oxidative stress-suppressing effects (Fig. 2). The derivatives showing small IC_{50} values for lipid peroxidation inhibitory activity, such as **3d**, **3–j**, tended to exhibit a strong intracellular oxidative stress-suppressing effect. Derivative **2** and uric acid did not show the effect. Similar to the lipid peroxidation inhibitory assay, the inactivity of these compounds was likely a result of their low lipophilicity and inability to penetrate the cell membrane.

The present results showed that the intracellular antioxidant effect of **1** could help to explain the results from a previous report by Cane et al., which determined that **1** decreased ERK2 phosphorylation.[16] ERK2 is a typical mitogen-activated protein kinase (MAPK), and its phosphorylation causes cell proliferation and differentiation. Oxidative stress was one of the inducers for ERK2 phosphorylation in various cells such as rat pleural mesothelial cells, hepatocytes, lung fibroblasts and astrocytes.[22–24] Cane et al. also revealed that 5-hydroxy-2-oxindole **1** showed antiproliferative

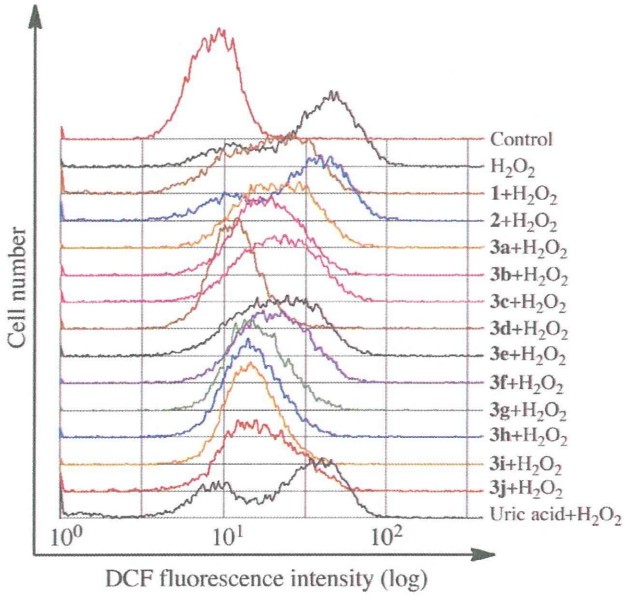

Figure 2. Intracellular oxidative stress suppressing effect HL60 cells (1.0×10^6 cells/well) were pre-treated with DCFH-DA (10 μM) for 15 min. Then, the cells were washed with phosphate buffered saline(−), followed by pre-incubation with the test compounds (10 μM) for 1 h. H_2O_2 (200 μM) was then added to the cells, followed by incubation for 1 h. The fluorescence intensity was measured with a flow cytometer.

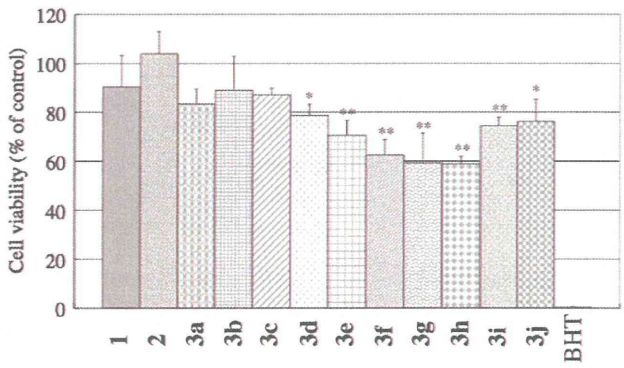

Figure 3. Cytotoxicity in HL60 The concentration of the test compound was 100 μM. Test compounds were incubated with HL60 (1.0×10^6 cell/well) for 24 h; then, the number of viable cells was counted using a trypan blue dye exclusion test ($n = 3$). The cell viability was expressed relative to the vehicle control (DMSO only) group (*P <0.05 vs **1**, **P <0.01 vs **1**, Student's t-test).

activity against the HL60, PC12, N1E-115, BALB/c3T3 and BBC cell lines, but 2-oxindole proved to be inactive.[16] In our previous report, we also found that 2-oxindole was inactive with respect to DPPH radical scavenging activity.[12] It was speculated that the inhibition of ERK2 phosphorylation by **1** was dependent on its radical scavenging activity. Intracellular antioxidative compounds **3a–j** were also expected to have ERK2 phosphorylation inhibitory activity and may be effectively utilized in ERK2-related investigations, such as those concerning β-amyloid induced neuronal toxicity.[25]

Compound **1** did not show cytotoxicity in HL60 cells at 100 μM (Fig. 3). Derivatives **2**, **3–c** also did not show cytotoxicity, but derivatives **3d–j** slightly decreased the cell viability at 100 μM. There was no correlation between the cytotoxicity and lipophilicity because the derivative **3b**, which showed moderate lipophilicity among the oxindoles, showed almost no cytotoxicity at 100 μM. BHT, a food additive that is generally recognized as safe (GRAS) by the US Food and Drug Administration (FDA),[26] showed high cytotoxicity. These data suggest that the cytotoxicity of the oxindole derivatives is inconsequential. Derivatives **3a–j** showed intracellular oxidative stress-suppressing effects at just 10 μM, so the beneficial effects of **3a–j** were observed at concentrations much lower than the levels that cause toxicity.

4. Conclusion

In conclusion, 5-hydroxyoxindole **1** and its 3-hydroxy-3-phenacyl derivatives showed effective antioxidant activity against lipid peroxidation and intracellular oxidative stress. Notably, the oxindole derivatives with appropriate lipophilicities, such as **3d**, **h** and **i**, showed remarkably potent antioxidant effects without cytotoxicity. Although the DPPH radical scavenging activity decreased, substitution at the C3-position of **1** seemed to be an effective modification for increasing the antioxidant activity in biological components. Our findings could be useful in the development of novel antioxidative medicine.

5. Experimental

5.1. Materials

^{1}H NMR spectra (500 MHz) were measured on a varian 500 FT-NMR with tetramethylsilane as an internal standard (δ = 0.00) in CD3OD or DMSO-d_6. ^{13}C NMR spectra (125 MHz) were obtained on the same spectrometer and the chemical shifts were referenced to the signals of CD_3OD (δ = 49.0) or DMSO-d_6 (δ = 39.5) or tetrahydrofuran-d_8 (δ = 25.5). Mass spectra were recorded on a JEOL JMS-700 mass spectrometer. Melting points were determined using a Yanagimoto MP-J3 micro-melting point apparatus and uncorrected. Column chromatography was performed using Merck Silica gel 60. 5-Hydroxyoxindole (**1**) was purchased from Apin Chemical Co. Hydrobromic acid, 5-methoxyisatin, diethylamine, 1,1-diphenyl-2-picrylhydrazyl, 2,6-di(*tert*-butyl)-4-hydroxytoluene and uric acid were purchased from Tokyo Kasei Kogyo Co. Ethanol and hydrogen peroxide (30%) were purchased from Wako Pure Chemical Co. RPMI-1640 medium, penicilline-streptomycin solution and 2′,7′-dichlorodihydrofluorescin diacetate were purchased from Sigma Inc. Heat-inactivated fatal bovine serum was purchased from Life Technologies, Co. Dimethyl sulfoxide (DMSO) was purchased from Aldrich Chemical Co.

5.2. Chemistry

5.2.1. Synthesis of 5-hydroxyisatin

5-Methoxyisatin (2.00 g, 11.2 mmol) was dissolved into 47% hydrobromic acid (20 mL) and refluxed at 150 °C for 3 h. The solution was diluted with water (100 mL) and extracted by ethyl acetate (300 mL × 5). The organic layers were combined and dried with anhydrous sodium sulfate. After concentration in vacuo, the crude dark-brown solid (1.64 g, 89% yield) was obtained. In the subsequent synthesis, 5-hydroxyisatin was used without further purification. ^{1}H NMR (CD_3OD, 500 MHz) δ 6.78 (d, 1H, J = 8.3 Hz, H-7), 6.94 (d, 1H, J = 2.4 Hz, H-4), 7.02 (dd, 1H, J = 8.3, 2.4 Hz, H-6).

5.2.2. Synthesis of 3-acetonyl-3,5-dihydoroxy-2-oxindole (2)

The crude 5-hydroxyisatin (200 mg, 1.22 mmol) was dissolved into acetone (20 mL) followed by addition of diethylamine (446 mg, 5.2 equiv). The reaction mixture was stirred at room temperature for 1 h. The solvent was evaporated under reduced pressure and the residue was purified with silica-gel column chromatography (*n*-hexane/ethyl acetate = 2:1–2:3) to give 127 mg of **2** as a light-yellow solid (47% yield). Recrystallization from chloroform/methanol yielded yellow plates. ^{1}H NMR (CD_3OD, 500 MHz) δ 2.08 (s, 3H, $-COCH_3$) 3.11 (d, 1H, J = 16.5 Hz, $-CH_2CO-$), 3.28 (d, 1H, J = 16.5 Hz, $-CH_2CO-$), 6.66 (dd, 1H, J = 8.3, 2.4 Hz, H-6), 6.70 (dd, 1H, J = 8.3 Hz, H-7), 6.81 (d, 1H, J = 2.4 Hz, H-4). ^{13}C NMR (CD_3OD, 125 MHz) δ 30.78, 51.14, 75.26, 111.77, 112.87, 116.59, 133.38, 135.51, 154.49, 181.08, 207.42. FAB-HRMS: calcd for $C_{16}H_{13}NO_4$ 221.0688, found 221.0670. Mp 164.8–166.9 °C (decomp.).

5.2.3. Synthesis of 3,5-dihydroxy-3-phenacyl-2-oxindole derivatives

5.2.3.1. General procedure. The crude 5-hydroxyisatin (200 mg, 1.22 mmol) was dissolved into methanol (20 mL) followed by addition of corresponding *para*-substituted acetophenone (5.0 equiv) and diethylamine (446 mg, 5.2 equiv). The reaction mixture was stirred at room temperature for 1 h. Then methanol and diethylamine were evaporated under reduced pressure. The dark-colored crude product was purified with silica-gel column chromatography (*n*-hexane/ethyl acetate = 2:1–2:3). All the synthetic oxindole derivatives were recrystallized before applying to biological study.

5.2.3.2. 3,5-Dihydroxy-3-phenacyl-2-oxindole (3a). The red-brown solid (255 mg, 74% yield) was obtained. Recrystallization from ethyl acetate yielded red-brown plates. ^{1}H NMR (CD_3OD, 500 MHz) δ 3.66 (d, 1H, J = 17.2 Hz, $-CH_2CO-$), 3.96 (d, 1H, J = 17.2 Hz, $-CH_2CO-$), 6.65 (dd, 1H, J = 8.3, 2.5 Hz, H-6), 6.73 (d, 1H, J = 8.3 Hz, H-7), 6.80 (d, 1H, J = 2.5 Hz, H-4), 7.44–7.48 (m, 2H, $-C_6H_5$) 7.56–7.60 (m, 1H, $-C_6H_5$), 7.89–7.91 (m, 2H, $-C_6H_5$). ^{13}C NMR (CD_3OD, 125 MHz) δ 46.73, 75.64, 111.75, 112.81, 116.52, 129.13, 129.73, 133.57, 134.55, 135.92, 137.96, 154.38, 181.34, 198.22. FAB-HRMS: calcd for $C_{16}H_{13}NO_4$ 283.0845, found 283.0872. Mp 194.5–196.2 °C (decomp.).

5.2.3.3. 3,5-Dihydroxy-3-(4′-methylphenacyl)-2-oxindole (3b). The light-yellow solid (135 mg, 37% yield) was obtained. Recrytallization from ethyl acetate yielded light-orange plates. ^{1}H NMR (CD_3OD, 500 MHz) δ 2.36 (s, 3H, $-CH_3$), 3.62 (d, 1H, J = 17.1 Hz, $-CH_2CO-$), 3.93 (d, 1H, J = 17.1 Hz, $-CH_2CO-$), 6.65 (dd, 1H, J = 8.3, 2.4 Hz, H-6), 6.73 (d, 1H, J = 8.3 Hz, H-7), 6.79 (d, 1H, J = 2.4 Hz, H-4), 7.26 (d, 2H, J = 7.9 Hz, $-C_6H_4CH_3$), 7.79 (d, 2H, J = 8.3 Hz, $-C_6H_4CH_3$). ^{13}C NMR (CD_3OD, 125 MHz) δ 21.58, 46.58, 75.66, 111.72, 112.78, 116.48, 129.28, 130.32, 133.60, 135.45, 135.89, 145.73, 154.33, 181.14, 197.88. FAB-HRMS: calcd for $C_{17}H_{15}NO_4$ 297.1001, found 297.0995. Mp 191.9–192.6 °C (decomp.).

5.2.3.4. 3,5-Dihydroxy-3-(4′-methoxyphenacyl)-2-oxindole (3c). The light-yellow solid (225 mg, 57% yield) was obtained. Recrystallization from ethyl acetate yielded light-yellow needless. ^{1}H NMR (CD_3OD, 500 MHz) δ 3.59 (d, 1H, J = 16.9 Hz, $-CH_2CO-$), 3.90 (d, 1H, J = 16.9 Hz, $-CH_2CO-$), 3.83 (s, 3H, $-OCH_3$), 6.64 (dd,

1H, J = 8.3, 2.5 Hz, H-6), 6.72 (d, 1H, J = 8.3 Hz, H-7), 6.79 (d, 1H, J = 2.5 Hz, H-4), 6.95–6.98 (m, 2H, $C_6H_4OCH_3$), 7.87–7.90 (m, 2H, $C_6H_4OCH_3$). ^{13}C NMR (CD_3OD, 125 MHz) δ 46.32, 56.04, 75.75, 111.70, 112.82, 114.86, 116.46, 130.89, 131.57, 133.66, 135.88, 154.33, 165.51, 181.40, 196.88. FAB-HRMS: calcd for $C_{17}H_{15}NO_5$ 313.0950, found 313.0946. Mp 187.5–188.6 °C (decomp.).

5.2.3.5. 3,5-Dihydroxy-3-(4′-nitrophenacyl)-2-oxindole (3d). The yellow solid (142 mg, 36% yield) was obtained. Recrystallization from ethyl acetate/*n*-hexane yielded light-yellow needles. ^{1}H NMR (CD_3OD, 500 MHz) δ 3.67 (d, 1H, J = 16.9 Hz, –CH_2CO–), 4.00 (d, 1H, J = 16.9 Hz, –CH_2CO–), 6.65 (dd, 1H, J = 8.3, 2.5 Hz, H-6), 6.72 (d, 1H, J = 8.3 Hz, H-7), 6.80 (d, 1H, J = 2.5 Hz, H-4), 8.10–8.12 (m, 2H, $C_6H_4NO_2$), 8.29–8.31 (m, 2H, $C_6H_4NO_2$). ^{13}C NMR (CD_3OD, 125 MHz) δ 47.27, 75.61, 111.79, 112.98, 116.62, 124.73, 130.45, 133.25, 135.74, 142.49, 151.87, 154.44, 181.06, 196.84. FAB-HRMS: calcd for $C_{16}H_{12}N_2O_6$ 328.0695, found 328.0720. Mp161.2–163.0 °C (decomp.).

5.2.3.6. 3-(4′-Cyanophenacyl)-3,5-dihydroxy-2-oxindole (3e). The light-yellow solid (157 mg, 42% yield) was obtained. Recrystallization from ethyl acetate/*n*-hexane yielded brown needles. ^{1}H NMR (CD_3OD, 500 MHz) δ 3.64 (d, 1H, J = 17.1 Hz, –CH_2CO–), 3.97 (d, 1H, J = 16.9 Hz, –CH_2CO–), 6.64 (dd, 1H, J = 8.3, 2.4 Hz, H-6), 6.71 (d, 1H, J = 8.3 Hz, H-7), 6.79 (d, 1H, J = 2.4 Hz, H-4), 7.83 (d, 2H, J = 8.5 Hz, C_6H_4CN), 8.04 (d, 2H, J = 8.5 Hz, C_6H_4CN). ^{13}C NMR (DMSO-d_6, 125 MHz) δ 46.04, 73.48, 109.80, 111.96, 114.76, 115.24, 118.12, 128.61, 132.43, 132.72, 134.36, 139.38, 152.28, 177.92, 196.02. FAB-HRMS: calcd for $C_{17}H_{12}N_2O_4$ 308.0797, found 308.0805. Mp 130.0–131.2 °C (decomp.).

5.2.3.7. 3-(4′-Fluorophenacyl)-3,5-dihydroxy-2-oxindole (3f). The light-yellow solid (230 mg, 63% yield) was obtained. Recrystallization from ethyl acetate/*n*-hexane yielded light-orange plates. ^{1}H NMR (CD_3OD, 500 MHz) δ 3.63 (d, 1H, J = 17.0 Hz, –CH_2CO–), 3.94 (d, 1H, J = 17.0 Hz, –CH_2CO–), 6.65 (dd, 1H, J = 8.3, 2.4 Hz, H-6), 6.72 (d, 1H, J = 8.3 Hz, H-7), 6.80 (d, 1H, J = 2.4 Hz, H-4), 7.15–7.19 (m, 2H, C_6H_4F), 7.96–7.99 (m, 2H, C_6H_4F). ^{13}C NMR (CD_3OD, 125 MHz) δ 46.65, 75.65, 111.75, 112.86, 116.58, 132.11, 133.49, 134.57, 135.84, 154.36, 166.31, 168.33, 181.27, 196.62. FAB-HRMS: calcd for $C_{16}H_{12}FNO_4$ 301.0750, found 301.0741. Mp 187.0–188.9 °C (decomp.).

5.2.3.8. 3-(4′-Chlorophenacyl)-3,5-dihydroxy-2-oxindole (3g). The light-yellow solid (219 mg, 57% yield) was obtained. Recrystallization from ethyl acetate/*n*-hexane yielded light-brown needles. ^{1}H NMR (CD_3OD, 500 MHz) δ 3.62 (d, 1H, J = 17.0 Hz, –CH_2CO–), 3.93 (d, 1H, J = 17.0 Hz, –CH_2CO–), 6.65 (dd, 1H, J = 8.4, 2.4 Hz, H-6), 6.72 (d, 1H, J = 8.4 Hz, H-7), 6.80 (d, 1H, J = 2.4 Hz, H-4), 7.45–7.48 (m, 2H, C_6H_4Cl), 7.87–7.90 (m, 2H, C_6H_4Cl). ^{13}C NMR (CD_3OD, 125 MHz) δ 46.72, 75.62, 111.75, 112.88, 116.56, 129.93, 130.85, 133.44, 135.83, 136.50, 140.78, 154.38, 181.23, 196.96. FAB-HRMS: calcd for $C_{16}H_{12}ClNO_4$ 317.0455, found 317.0450. Mp 166.5–168.0 °C (decomp.).

5.2.3.9. 3-(4′-Bromophenacyl)-3,5-dihydroxy-2-oxindole (3h). The light-yellow solid (248 mg, 57% yiled) was obtained. Recrystallization from ethyl acetate/*n*-hexane yielded light-brown needles. ^{1}H NMR (CD_3OD, 500 MHz) δ 3.61 (d, 1H, J = 17.0 Hz, –CH_2CO–), 3.92 (d, 1H, J = 17.0 Hz, –CH_2CO–), 6.65 (dd, 1H, J = 8.3, 2.4 Hz, H-6), 6.72 (d, 1H, J = 8.3 Hz, H-7), 6.79 (d, 1H, J = 2.4 Hz, H-4), 7.62–7.65 (m, 2H, C_6H_4Br), 7.80–7.82 (m, 2H, C_6H_4Br). ^{13}C NMR (CD_3OD, 125 MHz) δ 46.70, 75.62, 111.76, 112.88, 116.56, 129.42, 130.93, 133.00, 133.44, 135.83, 136.88, 154.39, 181.23, 197.16. FAB-HRMS: calcd for $C_{16}H_{12}BrNO_4$ 360.9932, found 360.9950. Mp 190.5–192.1 °C (decomp.).

5.2.3.10. 3,5-Dihydroxy-3-(4′-iodophenacyl)-2-oxindole (3i). The light-yellow solid (205 mg, 42% yield) was obtained. Recrystallization from ethyl acetate/*n*-hexane yielded light-brown needles. ^{1}H NMR (CD_3OD, 500 MHz) δ 3.60 (d, 1H, J = 17.1 Hz, –CH_2CO–), 3.91 (d, 1H, J = 17.1 Hz, –CH_2CO–), 6.65 (dd, 1H, J = 8.3, 2.4 Hz, H-6), 6.72 (d, 1H, J = 8.3 Hz, H-7), 6.79 (d, 1H, J = 2.4 Hz, H-4), 7.64 (d, 2H, J = 8.6 Hz, C_6H_4I), 7.95 (d, 2H, J = 8.6 Hz, C_6H_4I). ^{13}C NMR (CD_3OD, 125 MHz) δ 46.63, 75.60, 102,10, 111.75, 112.87, 116.55, 130.63, 133.44, 135.83, 137.31, 139.16, 154.38, 181.23, 197.49. FAB-HRMS: calcd for $C_{16}H_{12}INO_4$ 408.9831, found 408.9811. Mp 184.6–185.5 °C (decomp.).

5.2.3.11. 3,5-Dihydroxy-3-[4′-(trifluoromethyl)phenacyl]-2-oxindole (3j). The light-yellow solid (131 mg, 31% yield) was obtained. Recrystallization from ethyl acetate/*n*-hexane yielded light-brown needles. ^{1}H NMR (CD_3OD, 500 MHz) δ 3.68 (d, 1H, J = 17.1 Hz, –CH_2CO–), 3.99 (d, 1H, J = 17.1 Hz, –CH_2CO–), 6.65 (dd, 1H, J = 8.3, 2.4 Hz, H-6), 6.73 (d, 1H, J = 8.6 Hz, H-7), 6.81 (d, 1H, J = 2.4 Hz, H-4), 7.77 (d, 2H, J = 8.3 Hz, $C_6H_4CF_3$), 8.07 (d, 2H, J = 8.3 Hz, $C_6H_4CF_3$). ^{13}C NMR (tetrahydrofuran-d_8, 125 MHz) δ 46.85, 74.71, 111.24, 113.09, 115.64, 126.17, 129.63, 133.62, 134.27, 134.53, 135.80, 141.24, 153.85, 178.74, 196.24. FAB-HRMS: calcd for $C_{17}H_{12}F_3NO_4$ 351.0718, found 351.0725, Mp 174.4–175.8 °C (decomp.).

5.3. Measurement of logK_w value

The measurement procedure was used the method in our previous report with some modification.[20] Sample was dissolved into acetonitrile/acetone = 99:1 mixture. The mobile phase was made up volumetrically by distilled water and different proportions of methanol in the range of 5–55%. Two microliters of sample solution was injected on an octadecyl-silicagel-prepacked column Prodigy-3 5 μM ODS (150 mm × 4.8 mm, Phenomenex Inc.) and eluted with a flow rate of 1.0 mL/min. Compounds **1**, **2**, **3a–j** and acetone were detected at 254 nm with a Shimadzu SPD-10A UV–vis detector. Isocratic capacity factors, defined as $\log[(t_r - t_o/t_0)]$, were linearly extrapolated to 0% methanol to yield $\log k_w$ (t_r: retention time of the tested compounds, t_0: retention time of unretained acetone).

5.4. DPPH radical scavenging activity

The assay protocol of Yamaji et al.[27] was used with some modification. DPPH (12.5 μM) was dissolved into the mixed solution of 41.8 mM 4-morpholinoethanesulfonic acid (MES) buffer (pH 7.4) and ethanol (2/3, v/v). The test compounds (0.25, 0.50, 0.75 and 1.00 mM) were dissolved into the mixed solution of MES buffer (pH 7.4) and ethanol (3/2, v/v). The stock solution of the test compounds (200 μL) and DPPH (200 μL) were mixed automatically with a UNISOKU Rapid-Scan Stopped-Flow Spectoroscopy System RSP-1000 and the decrease in the optical absorbance of DPPH at 517 nm was measured. The pseudo first-order rate constant was calculated from the obtained curve with a UNISOKU Spectoroscopy and Kinetics. The obtained pseudo-first order rate constants were plotted against the concentration of test compounds and the second-order rate constant was obtained from the slope of regression line. In our previous report,[12] the second-order rate constant was directly calculated based on a decreasing curve by fitting method using a UNISOKU Spectroscopy & Kinetics. We assume that there is no significant difference between the previous and present experimental processes and obtained values, but the present method would be more reliable.